

ArrayBot: Reinforcement Learning for Generalizable Distributed Manipulation through Touch

Zhengrong Xue^{*1,2,3,4}, Han Zhang^{*1,2}, Jingwen Cheng¹, Zhengmao He²,
Yuanchen Ju^{1,5}, Changyi Lin², Gu Zhang^{2,4}, Huazhe Xu^{†1,2,3}

¹Tsinghua University, ²Shanghai Qi Zhi Institute, ³Shanghai AI Lab,
⁴Shanghai Jiao Tong University, ⁵Southwest University

<https://steven-xzr.github.io/ArrayBot>

Abstract: We present ArrayBot, a distributed manipulation system consisting of a 16×16 array of vertically sliding pillars integrated with tactile sensors, which can simultaneously support, perceive, and manipulate the tabletop objects. Towards generalizable distributed manipulation, we leverage reinforcement learning (RL) algorithms for the automatic discovery of control policies. In the face of the massively redundant actions, we propose to reshape the action space by considering the spatially local action patch and the low-frequency actions in the frequency domain. With this reshaped action space, we train RL agents that can relocate diverse objects through tactile observations only. Surprisingly, we find that the discovered policy can not only generalize to unseen object shapes in the simulator but also transfer to the physical robot without any domain randomization. Leveraging the deployed policy, we present abundant real-world manipulation tasks, illustrating the vast potential of RL on ArrayBot for distributed manipulation.

Keywords: Distributed Manipulation, Reinforcement Learning, Tactile Sensing

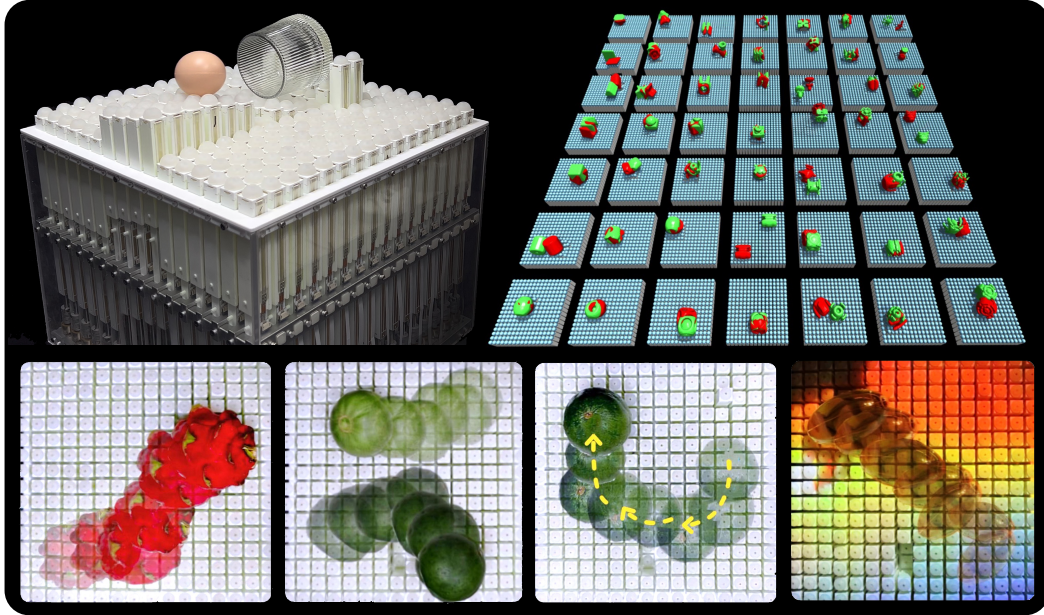


Figure 1: We design and manufacture the hardware of ArrayBot, a distributed manipulation system. Towards generalizable distributed manipulation, we train reinforcement learning (RL) agents on the simulated ArrayBot where the only accessible observation is the tactile information. We deploy the control policy to the physical robot and showcase the bird’s-eye view of the trajectories for real-world manipulation tasks: relocating objects of novel shapes, manipulation in parallel, trajectory following, and manipulating transparent objects under severe visual disturbance.

^{*}Equal Contribution. [†]Corresponding Author. Contact: huazhe_xu@mail.tsinghua.edu.cn

1 Introduction

The notion of robotic manipulation [1, 2] easily invokes the image of a biomimetic robot arm or hand trying to grasp tabletop objects and then rearrange them into desired configurations inferred by exteroceptive sensors such as RGBD cameras. To facilitate this manipulation pipeline, the robot learning community has made tremendous efforts in either how to determine steadier grasping poses in demanding scenarios [3, 4, 5, 6, 7] or how to understand the exteroceptive inputs in a more robust and generalizable way [8, 9, 10, 11, 12, 13]. Acknowledging these progresses, this paper attempts to bypass the challenges in the prevailing pipeline by advocating ArrayBot, a reinforcement learning driven system for distributed manipulation [14], where the objects are manipulated through a great number of actuators with only proprioceptive tactile sensing [15, 16, 17, 18].

Conceptually, the hardware of ArrayBot is a 16×16 array of vertically sliding pillars, each of which can be independently actuated, leading to a 16×16 action space. Functionally, the actuators beneath a tabletop object can support its weight and at the same time cooperate to lift, tilt, and even translate it through proper motion policies. To equip ArrayBot with proprioceptive sensing, we integrate each actuator with a slim and low-cost Force Sensing Resistor (FSR) sensor, allowing the robot to “feel” the object when lack of external visual inputs. Thanks to its distributed nature, ArrayBot is flexible in size, inherently supports manipulation in parallel, and has the potential to manipulate objects times larger than the size of its end-effector.

Previous works for distributed manipulation show up in the names of actuator array [19, 20, 21, 22], smart surface [23, 24], or auxiliary functions of tangible user interface [25, 26, 27]. Despite their promises to manipulate tabletop objects, they heavily depend on pre-defined motion primitives to fit the specific designs of the actuators and could only manipulate fixed types of objects in a pre-programmed manner, which hinders their usefulness in actual applications. Towards distributed manipulation enjoying better generalizability and versatility, we explore the feasibility of applying model-free reinforcement learning (RL) [28, 29, 30] to the automatic discovery of control policies. However, compared with popular manipulators such as arms or hands, controlling ArrayBot in its 2D-array action space can be extremely challenging because the massive redundancy of the actions makes the trial-and-error process hopelessly inefficient.

In awareness of its redundancy, we propose to reshape the action space with the objective to strengthen its inductive bias towards more favorable actions for distributed manipulation. To start with, we explicitly restrict the extend of the valid action space to the *local action patch* centered around the object since far away actuators could hardly exert any physical effect. Meanwhile, we propose the idea of considering *actions in the frequency domain* via 2D Discrete Cosine Transform (DCT) [31]. The rationale is that for distributed manipulation, the impacts of *collective* behaviors are more stable and predictable than *individual* collisions [32, 33]. As each channel in the frequency domain processes a spatially global horizon, an action space in the frequency domain may enjoy an implicit bias toward collaborations. On top of the frequency transform, we further perform *high frequency truncation* on the action channels, which is inspired by image compression methods such as JPEG [34] that discard high-frequency patterns. Likewise, we argue the same preference applies to the 2D-array action space because lower-frequency actions are likely to produce emergent motion primitives with semantics, e.g., the DC channel implies lifting, and the base frequency implies tilting. In contrast, the detailed texture information determined by higher-frequency channels makes little influence on the manipulation tasks.

With the reshaped action space, we first demonstrate that the policies discovered by model-free RL on ArrayBot are as capable as pre-defined primitives by setting up the ArrayBot environment in the Isaac Gym simulator [35] and then training RL agents [30] that lift and flip a cube respectively. Going beyond the reach of motion primitives, we showcase one single policy on ArrayBot learned by RL that is agnostic of both object shapes and visual observations, but could relocate hundreds of previously unseen objects of various shapes from and to arbitrary positions via touch sensing alone. Surprisingly, we find it possible to directly deploy the policy trained in the simulator to the real-world machine without any sim-to-real transfer techniques including domain randomization [36].

Leveraging the general relocate-via-touch policy deployed to the real world, we present some more concrete applications of ArrayBot showing its ability to manipulate objects of diverse shapes and drive objects according to specified trajectories, its robustness to dramatically varying environment appearances and transparent objects, and finally its potential for manipulation in parallel. We also present some hard-coded policies for very static but more complicated tasks to demonstrate the vast potential of our hardware. For visual impression, please refer to the [project website](#).

Our contributions are summarized as: (i) we design and manufacture the hardware of ArrayBot that could simultaneously support, perceive, and manipulate objects; (ii) we propose methods of action space reshaping for ArrayBot that validate the automatic policy discovery via model-free RL on a distributed manipulation system; (iii) we train one relocate-via-touch policy suitable for various shapes in the simulator which can be instantly deployed to the real world; (iv) we provide concrete applications empowered by the RL-derived policy to better illustrate the advantages of ArrayBot.

2 Action Space Reshaping for Distributed Manipulation

The central challenge against the employment of RL for distributed manipulation comes from its unconventional action space with massive redundancy. In this section, we present a series of techniques to reshape the action space of ArrayBot so that it is more favored for distributed manipulation.

Local action patch. The action space of ArrayBot is in the shape of a 16×16 array. Given the fact that the actuators far away from the object could not make any impact on manipulation, we only consider a 5×5 local action patch (LAP) centered around the object. So far, an untouched detail is how to determine the center of the local patch. If the ground-truth positions of the objects are assumed to be accessible in the simulator, we simply select the actuator that is closest to the center of the object as the center of the LAP. However, the observation space in a real-world scenario does not include such privileged state information. In ArrayBot, we estimate the object position through touch. More specifically, we post-process the noisy readings of the 16×16 FSR sensor array, giving a binary tactile map that indicates contact conditions. Afterward, the mean of the contact points is calculated as the estimated center position of the manipulated object.

Actions in the frequency domain. Rather than figure out the impact of every individual contact in a contact-rich environment which is virtually insolvable [32, 33], we instead consider the impacts of collective behaviors for distributed manipulation [26, 21, 22]. We propose to learn actions in the frequency domain in which each component may have a global impact in the spatial domain. Hence, rather than directly predict a flattened 25-dimensional variance of positions, the policy network outputs a 25-dimensional variance of frequencies. Subsequently, the 25-dimensional output is unflattened to the shape of 5×5 and then post-processed by a 2D inverse Discrete Cosine Transform (iDCT) [31] operator to produce the ultimate 5×5 action in the spatial domain.

High frequency truncation. Besides a latent inductive bias towards collaborations, the frequency domain also provides a valuable point of view to re-inspect the redundancy of the actions. Intuitively, low-frequency channels lead to smooth planar surfaces with semantics that are likely to correspond to emergent motion primitives. Based on these observations, we propose to truncate the high-frequency channels of the actions. The policy network is now designed to output a 6-dimensional prediction, which is used to fill the 6 lowest-frequency channels of the entire predicted action in the frequency domain. To acquire a full 25-dimensional action ready for the inverse frequency transform, we simply zero-pad the rest 19 channels of higher frequencies.

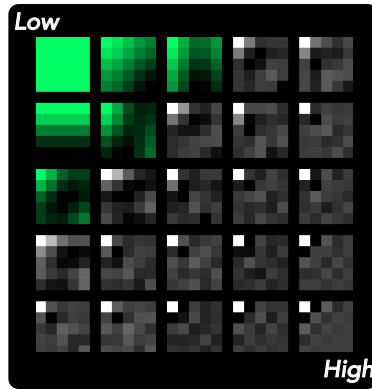


Figure 2: We consider the 6 lowest-frequency channels marked in green on a 5×5 2D DCT map.

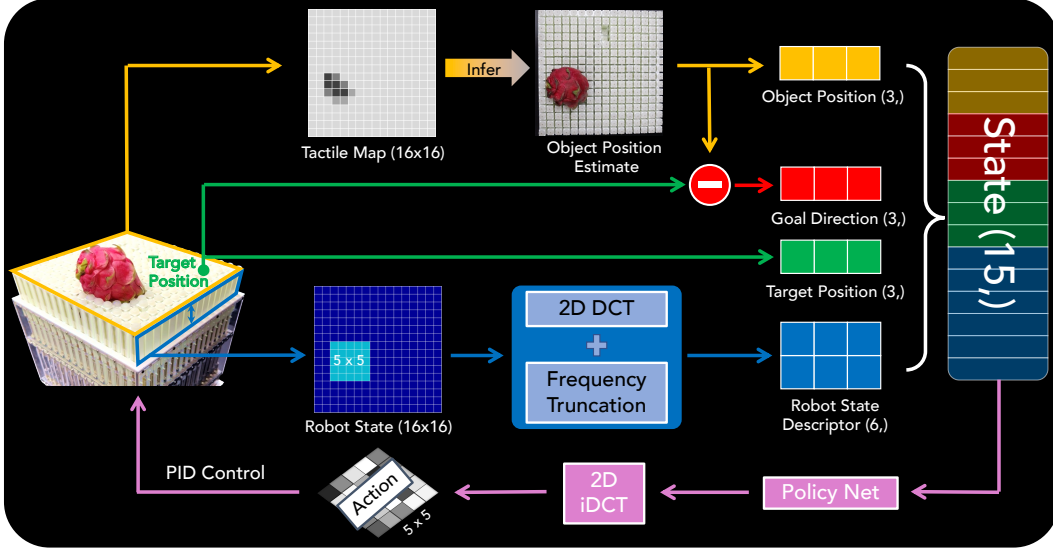


Figure 3: An overview of the RL framework on ArrayBot for *general relocation*. The state is the combination of the estimated object position, the specified target position, the residual goal direction, and the robot state in the frequency domain. Exempt from any visual inputs, the states are inferred from purely proprioceptive observations of the robot joint configuration and the tactile sensor array.

3 Learning Control Policies in the Reshaped Action Space

3.1 System Setup

The hardware. We design and manufacture the hardware of ArrayBot, which can be perceived as a 16×16 array of vertically sliding units. Each unit from down to up consists of a motor that drives the unit to move in the vertical direction, a rectangular pillar whose length of each dimension is $16 \times 16 \times 200$ mm respectively, a slim and low-cost Force Sensing Resistor (FSR) sensor that measures the vertical pressure, and a silicone hemispheric end-effector that protects the tactile sensor and increases the frictions. The effective range of each vertically prismatic joint is 55 mm, whose maximum speed of motion is 53 mm/s. Actions are executed by ArrayBot via positional PID control.

The simulator. The physical simulation of contact-rich interactions could be time-consuming. To produce sufficient samples in an efficient way so as to feed data-hungry RL algorithms, we build the simulated environment of ArrayBot in the Isaac Gym [35] simulator. The frequency of the physical simulation steps is 50 Hz. Due to the mechanical speed limit, we set the frequency of RL control to be 5 Hz. Since the RL algorithm considers the binarized outcome of the tactile sensor, we retrieve the information from the contact buffer of the simulator as the simulation of tactile sensors.

3.2 Environments

We consider three manipulation tasks: *lifting*, *flipping*, and *general relocation*. In *lifting*, we ask ArrayBot to raise a cubic block as high as possible. In *flipping*, we ask ArrayBot to flip the same block by 90 degrees along a certain axis. In *general relocation*, we ask ArrayBot to relocate objects of various shapes from and to any arbitrary positions within its reach via only tactile sensing.

States. The tasks of *lifting* and *flipping* directly make use of the privileged position and orientation information provided by the simulator. In *general relocation*, we consider a more realistic scenario where the only observation is the binarized tactile information. The estimated states for *general relocation* are visualized in Figure 3. More details can be found in Table 1 in Appendix B.

Rewards. The tasks of *lifting* and *flipping* simply consider a dense reward of object height and orientation respectively. In *general relocation*, apart from the dense reward of object position, we

add one more sparse bonus reward when reaching the goal that would encourage the robot to timely stop the object at the goal position. More details can be found in Table 2 in Appendix B.

Actions. At each step, the policy outputs a 6-dimensional action in the frequency domain, which is post-processed to produce the relative joint configuration on the 5×5 LAP.

Resets. We reset the episode if the tabletop object moves out of the border or the episode length reaches 100 steps. With the existence of the 5×5 LAP, we request that the center of the object should locate on the central 11×11 patch.

Manipulated objects. In *lifting* and *flipping*, we manipulate an $8 \times 8 \times 8$ cm cubic block which can be roughly supported by a 4×4 array of actuators. In *general relocation*, we train an RL agent that is generalizable to shape variance by sampling 128 different shapes from the EGAD [37] training set and then re-scaling them. At test time, we evaluate the performance of the generalizable agent on the EGAD test set with a total of 49 unseen object shapes. For fast and accurate collision detection in the simulator, we perform V-HACD [38] convex decomposition to all of the object shapes.

3.3 Training RL agents

For all the tasks, we train proximal policy optimization (PPO) [30] agents on 128 parallel Isaac Gym environments for the automatic discovery of control policies. More details in RL training can be found in Appendix B. Notably, all of the 128 parallel environments for *general relocation* involve mutually different object shapes. With a state space agnostic of the object shapes at all, the agent receives mixed types of dynamics. This forces the agent to discover a policy that is as universal as possible for all the shapes in the dataset, thus enhancing its generalizability to the shape variance.

3.4 Experiments for Lifting and Flipping

Metrics. In *lifting* and *flipping*, we compare the averaged accumulated returns and the survival steps of each episode. The survival step refers to the steps an object could stay on the robot without falling. The survival step has a maximum of 100.

Compared methods. To study the necessity of our reshaped action space, we train the same PPO algorithm in the following action spaces: (i) *LAP only* in the spatial domain; (ii) *LAP+DCT-25* that preserves all of the 25 channels in the frequency domain; and (iii) *LAP+DCT-6* that considers only the 6 lowest-frequency channels.

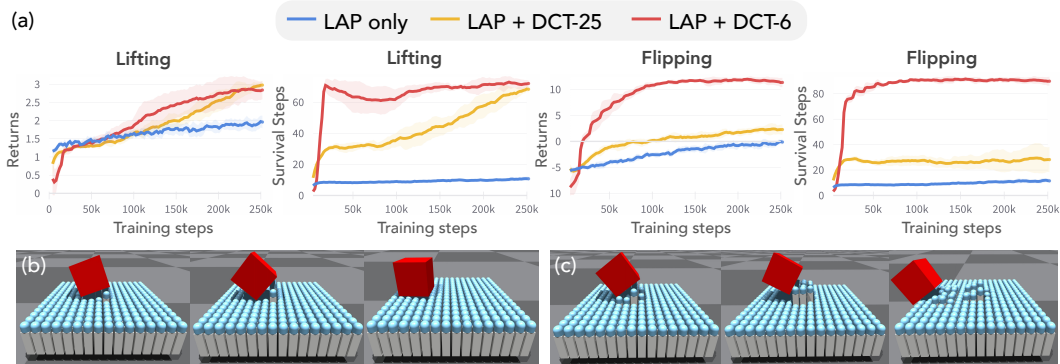


Figure 4: (a) The training curves in terms of episode returns and survival steps. The results are averaged on 5 seeds. The shaded area stands for the standard deviation. (b)(c) The example trajectories of the policies learned by (b) *LAP+DCT-6* and (c) *LAP only* for *flipping*.

Results. The learning curves of both tasks are shown in Figure 4(a). In both tasks, the DCT-based approaches have a significant advantage over the one trained in the spatial action space in terms of both total returns and survival steps. Further, the *DCT-6* method survives longer and behaves better than *DCT-25*, especially in the more challenging task of *flipping*, echoing the intuition that low-frequency patterns lead to more steady actions. By visualizing the *flipping* trajectories in Figure 4(b)(c), we find that *LAP only* hacks the environment and learns to gain rewards by throwing the block off the robot in a rolling way. In comparison, the actions of *LAP+DCT-6* are more gentle and reasonable, which explains its better performance and longer survival time.

3.5 Experiments for General Relocation

Metrics. We report the success rate of relocation on the EGAD [37] test set containing 49 unseen objects. An episode is judged to succeed if the object reaches the target position and insists for at least 1 second. The results are averaged over 200 trails with random initial and target positions.

Results. The success rates shown in the right figure follow the same taxonomy in EGAD where the grasping difficulty and shape complexity of objects is alphabetically and numerically sorted. We observe that ArrayBot can achieve relatively high success rates on most of the low-difficulty objects even when the shape complexity is high. Considering none of the objects is shown to the RL agent at training time, this indicates remarkable generalizability. Meanwhile, we find that specific objects that are considered as hard to grasp (e.g., F3 & F4) are relatively easy for ArrayBot. This implies that ArrayBot might have complementary ability to the existing general manipulators. In the course of the evaluation, we find the control policy discovered by RL on ArrayBot is a mixture of sliding and rolling. This explains why slender planar objects (e.g., G6 is in the shape of a piece of snow), which pose significant difficulties for conventional grasping methods, also present challenges for distributed manipulation techniques due to their limited ability to undergo rolling motion.

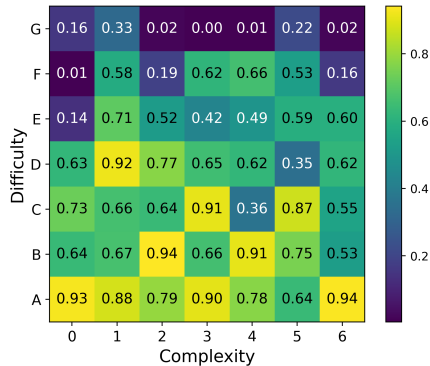


Figure 5: The success rate of the *general relocation* policy on the previously unseen EGAD [37] test set.

4 Deploying Control Policies to the Physical Robot

Zero-shot sim-to-real transfer. To our surprise, we find that the general relocation policy trained on the EGAD dataset in the simulator can be effortlessly deployed to the physical robot for multiple relocation-based tasks. Note that the instant sim-to-real transfer even exempts the involvement of popular sim-to-real techniques such as domain randomization [36]. Intuitively, there are two sources of sim-to-real gaps: perception and dynamics. Our selection of proprioceptive observations and binarized tactile measurements keeps the discrepancies in perception at a low level. Meanwhile, both the diverse shapes introduced at training time and the massive redundancy in the action space contribute to the resilience towards the shift in dynamics. These factors combined explain the extraordinary convenience that ArrayBot brings in the sim-to-real procedure.

Real-world manipulation tasks. Leveraging the general relocation policy successfully deployed to the real world, we manage to further demonstrate the merits of our ArrayBot by presenting the following manipulation tasks on the physical robot:

- *Manipulating objects of diverse shapes.* ArrayBot is particularly good at natural objects such as melons and dragon fruits. It could also manipulate man-made objects such as rubber duck and rugby-shaped artware. Note that the objects are times larger than the size of the end-effector, which is beyond the reach of arms or hands since they are too large to grasp or hold.

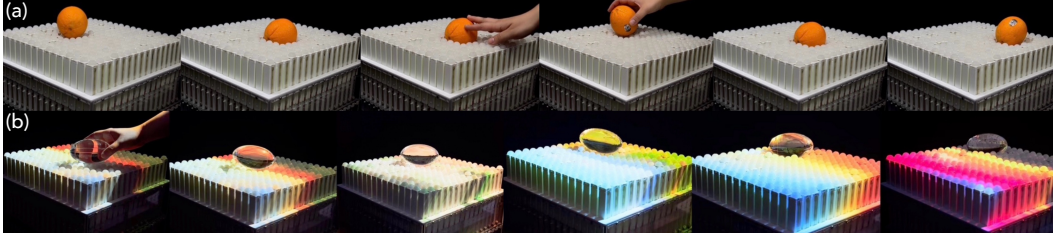


Figure 6: Real-world trajectories of the manipulation tasks showing the robustness of our system to the impacts of (a) unexpected external forces (b) severe visual degradations.

- *Trajectory following.* Trajectory following can be easily achieved by iterative calls of the general relocation policy. Note that ArrayBot is friendly to incremental operations since its efforts are in proportion to the traveled distance. In comparison, slight operations are as troublesome for arms or hands since the costs in “pick” and “place” are constants whatever the scale of the operations.
- *Manipulation in parallel.* Consisting of a large number of actuators, ArrayBot inherently supports parallel manipulation. Thanks to the spatial self-similarity in the mechanical structure, the same control policy automatically adapts to all local patches. Assuming no collision occurs, manipulating two objects in parallel is as easy as initializing two independent processes for manipulation. We leave more complicated collision-involved parallel manipulation for future work.
- *Manipulation under visual degradations.* Relying on no visual observations at all, ArrayBot is no doubt robust to visual degradations. We exhibit the ability of ArrayBot to confidently manipulate transparent objects under severe visual disturbance from a projector.

Besides the power of RL-derived control policies, we also showcase some hard-coded policies for static but more complicated manipulation settings. For visual illustration of the aforementioned tasks, please find Figure 1&6, Figure 10&11 in Appendix C, and the [project website](#).

5 A Sketch for the Hardware Design

ArrayBot consists of a robotic frame and densely arranged controllable pillars. The robotic frame is composed of supporting aluminum alloy columns, acrylic plates, and a stainless steel base. Inside the frame, there are 256 rectangular prism pillars that can move vertically powered by motor drives under the constraints of sliding rail brackets. Each pillar has a cross-sectional area of $16 \times 16 \text{ mm}^2$ and needs to be compactly arranged with gaps of 4 mm for smooth manipulation. The pillar movements are controlled by STM32 microcontrollers. In this section, we provide important hardware design choices of ArrayBot. We leave the full-fledged design details to Appendix A.

End-effector. The right side of Figure 7(a) is the end-effector, which has a silicone semi-spheric cap and an FSR tactile sensor. When an object is placed on the end effector, the supporting force is transmitted through the silicone cap to the plate-shaped FSR sensor. For successful signal transmission in limited physical space, we design a conductive sliding rail that can avoid the use of wires.

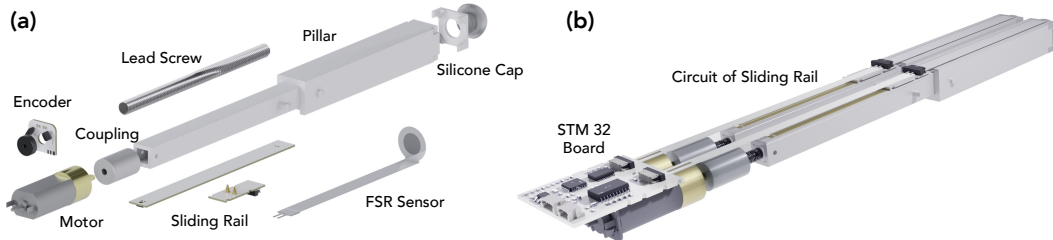


Figure 7: (a) The exploded view of a single pillar. (b) The assembled modular unit of a 1×2 array.

Actuators. The left side of Figure 7(a) is the actuator, which is a direct current (DC) gear motor. It converts the rotational motion of the motor into translational motion through a screw structure. A magnetic encoder is installed on the rotating shaft of the motor to calculate the angle and angular velocity and ultimately map them to the position and speed of the pillar.

Pillar module. As shown in Figure 7(b), in order to facilitate assembly and maximize the utilization of the microcontroller’s performance, we combine every two pillars into a module controlled by an STM32 board. Hence, the entire robot contains 128 modules that are controlled by 4 Controller Area Network (CAN) signals. During operation, the STM32 board receives the CAN commands from a desktop, processes them, and outputs two pulse width modulation (PWM) signals respectively to control the two motors.

6 Related Works

Distributed manipulation controls the motion of the target object through numerous points of contact [14]. Composed of an array of stationary unit cells, a distributed manipulation system is able to be scaled in size and inherently support manipulation in parallel. Reviewing the literature, the majority of distributed manipulation systems consist of an array of special-purpose actuators such as vibrating plates [19], air jets [39], roller wheels [20], electromagnets [25] and delta robots [21, 22]. While they are designed to be skilled in specific types of manipulation tasks, they are typically not versatile enough and demand elaborately pre-defined motion primitives. Compared with the prototypes in robotics research, the hardware of ArrayBot is more related to the branch of works known as the “shape-changing tangible user interfaces” [26, 27, 40] in the human-computer interface community, where the actuators are vertically prismatic pillars. The simplicity in design not only makes it easier to manufacture; its organized action space also helps open the door to learning motion policies with model-free RL.

Learning in the frequency domain is a widely discussed concept in a variety of scopes in the machine learning community. In computer vision studies, frequency transformations are adopted to bridge the gap between high-quality images and down-sampled ones [41], and help achieve more accurate gradient approximations in Binary CNNs [42]. In the topics of reinforcement learning, the concept of frequency is utilized to boost the efficiency of search-control in model-based architectures [43], and represent the characteristic function of returns for distributional RL [44]. In contrast to all the existing works that we have found, frequency transformation is leveraged in ArrayBot for action space reshaping, aiming at reformative sample efficiency in model-free RL.

7 Conclusion and Limitations

We present ArrayBot, an RL-driven distributed manipulation system with tactile sensing. We train a generalizable relocate-via-touch policy in the proposed reshaped action space, which can be instantly transferred to the physical robot. Leveraging the deployed policy, we showcase the distinctive merits of our ArrayBot through a variety of real-world manipulation tasks.

Given all our findings, we would like to call for the attention of the robot learning community to distributed manipulation. We believe the redundancy in its unconventional action space is a two-edged sword. As long as we find ways to alleviate its demon face of sample inefficiency, its angel face of fault tolerance might offer shortcuts for solving well-known challenges in the community such as generalizability to object shapes and bridging the sim-to-real gaps.

Admittedly, the prototype of ArrayBot is not yet perfect. For instance, its 16×16 size is still not large enough for large-scale multi-object manipulation in parallel. The speed limit of the joints may hinder the RL agent from exploring more highly dynamical control policies. We also find that the tactile sensors are sometimes not sensitive enough given that the pressure exerted by an object is shared by multiple sensors. In the future, we will continually upgrade both the hardware and software of ArrayBot so as to unearth the even greater potential of RL for distributed manipulation.

Acknowledgments

We would like to give special thanks to Mr. Yuanhong Wang and his group of colleagues from Kunshan Qiaotuo ModelTech Co., Ltd. for their contributions to the manufacture of the hardware. We also thank Yitong Wang for hardware maintenance, Tianyu Huang and Yao Lu for elegant graphic rendering of the hardware design, and Yuzhe Qin for his advice on the Isaac Gym simulator. Huazhe Xu is supported by National Key R&D Program of China (2022ZD0161700).

References

- [1] A. Billard and D. Kragic. Trends and challenges in robot manipulation. *Science*, 364(6446): eaat8414, 2019.
- [2] O. Kroemer, S. Niekum, and G. Konidaris. A review of robot learning for manipulation: Challenges, representations, and algorithms. *The Journal of Machine Learning Research*, 22(1):1395–1476, 2021.
- [3] J. Kerr, L. Fu, H. Huang, Y. Avigal, M. Tancik, J. Ichnowski, A. Kanazawa, and K. Goldberg. Evo-nerf: Evolving nerf for sequential robot grasping of transparent objects. In *6th Annual Conference on Robot Learning*.
- [4] W. Zhou and D. Held. Learning to grasp the ungraspable with emergent extrinsic dexterity. In *Conference on Robot Learning*, pages 150–160. PMLR, 2023.
- [5] X. Zhu, D. Wang, O. Biza, G. Su, R. Walters, and R. Platt. Sample efficient grasp learning using equivariant models. *arXiv preprint arXiv:2202.09468*, 2022.
- [6] L. Shao, F. Ferreira, M. Jorda, V. Nambiar, J. Luo, E. Solowjow, J. A. Ojea, O. Khatib, and J. Bohg. Unigrasp: Learning a unified model to grasp with multifingered robotic hands. *IEEE Robotics and Automation Letters*, 5(2):2286–2293, 2020.
- [7] J. W. James and N. F. Lepora. Slip detection for grasp stabilization with a multifingered tactile robot hand. *IEEE Transactions on Robotics*, 37(2):506–519, 2020.
- [8] R. Shi, Z. Xue, Y. You, and C. Lu. Skeleton merger: an unsupervised aligned keypoint detector. In *Proceedings of the IEEE/CVF conference on computer vision and pattern recognition*, pages 43–52, 2021.
- [9] W. Yuan, C. Paxton, K. Desingh, and D. Fox. Sornet: Spatial object-centric representations for sequential manipulation. In *Conference on Robot Learning*, pages 148–157. PMLR, 2022.
- [10] A. Simeonov, Y. Du, A. Tagliasacchi, J. B. Tenenbaum, A. Rodriguez, P. Agrawal, and V. Sitzmann. Neural descriptor fields: Se (3)-equivariant object representations for manipulation. In *2022 International Conference on Robotics and Automation (ICRA)*, pages 6394–6400. IEEE, 2022.
- [11] Z. Xue, Z. Yuan, J. Wang, X. Wang, Y. Gao, and H. Xu. Useek: Unsupervised se (3)-equivariant 3d keypoints for generalizable manipulation. *arXiv preprint arXiv:2209.13864*, 2022.
- [12] I. Radosavovic, T. Xiao, S. James, P. Abbeel, J. Malik, and T. Darrell. Real-world robot learning with masked visual pre-training. In *Conference on Robot Learning*, pages 416–426. PMLR, 2023.
- [13] B. Wen, W. Lian, K. Bekris, and S. Schaal. You only demonstrate once: Category-level manipulation from single visual demonstration. In *Robotics: Science and Systems (RSS)*, 2022.
- [14] K. F. Böhringer, H. Choset, and H. Choset. *Distributed manipulation*. Springer Science & Business Media, 2000.

- [15] G. Khandate, M. Haas-Heger, and M. Ciocarlie. On the feasibility of learning finger-gaiting in-hand manipulation with intrinsic sensing. In *2022 International Conference on Robotics and Automation (ICRA)*, pages 2752–2758. IEEE, 2022.
- [16] S. Pai, T. Chen, M. Tippur, E. Adelson, A. Gupta, and P. Agrawal. Tactofind: A tactile only system for object retrieval. *arXiv preprint arXiv:2303.13482*, 2023.
- [17] I. Guzey, B. Evans, S. Chintala, and L. Pinto. Dexterity from touch: Self-supervised pre-training of tactile representations with robotic play. *arXiv preprint arXiv:2303.12076*, 2023.
- [18] Z.-H. Yin, B. Huang, Y. Qin, Q. Chen, and X. Wang. Rotating without seeing: Towards in-hand dexterity through touch. *arXiv preprint arXiv:2303.10880*, 2023.
- [19] K.-F. Bohringer, V. Bhatt, and K. Y. Goldberg. Sensorless manipulation using transverse vibrations of a plate. In *Proceedings of 1995 IEEE International Conference on Robotics and Automation*, volume 2, pages 1989–1996. IEEE, 1995.
- [20] J. E. Luntz, W. Messner, and H. Choset. Distributed manipulation using discrete actuator arrays. *The International Journal of Robotics Research*, 20(7):553–583, 2001.
- [21] S. Thompson, P. Mannam, Z. Temel, and O. Kroemer. Towards robust planar translations using delta-manipulator arrays. In *2021 IEEE International Conference on Robotics and Automation (ICRA)*, pages 6563–6569. IEEE, 2021.
- [22] S. Patil, T. Tao, T. Hellebrekers, O. Kroemer, and F. Z. Temel. Linear delta arrays for dexterous distributed manipulation. *arXiv preprint arXiv:2206.04596*, 2022.
- [23] D. R. Barr, D. Walsh, and P. Dudek. A smart surface simulation environment. In *2013 IEEE International Conference on Systems, Man, and Cybernetics*, pages 4456–4461. IEEE, 2013.
- [24] T. A. T. Dang, M. Bosch-Mauchand, N. Arora, C. Prella, and J. Daaboul. Electromagnetic modular smart surface architecture and control in a microfactory context. *Computers in Industry*, 81:152–170, 2016.
- [25] G. Pangaro, D. Maynes-Aminzade, and H. Ishii. The actuated workbench: computer-controlled actuation in tabletop tangible interfaces. In *Proceedings of the 15th annual ACM symposium on User interface software and technology*, pages 181–190, 2002.
- [26] S. Follmer, D. Leithinger, A. Olwal, A. Hogge, and H. Ishii. inform: dynamic physical affordances and constraints through shape and object actuation. In *Uist*, volume 13, pages 2501–988. Citeseer, 2013.
- [27] D. Leithinger, S. Follmer, A. Olwal, and H. Ishii. Shape displays: Spatial interaction with dynamic physical form. *IEEE computer graphics and applications*, 35(5):5–11, 2015.
- [28] T. P. Lillicrap, J. J. Hunt, A. Pritzel, N. Heess, T. Erez, Y. Tassa, D. Silver, and D. Wierstra. Continuous control with deep reinforcement learning. *arXiv preprint arXiv:1509.02971*, 2015.
- [29] T. Haarnoja, A. Zhou, P. Abbeel, and S. Levine. Soft actor-critic: Off-policy maximum entropy deep reinforcement learning with a stochastic actor. In *International conference on machine learning*, pages 1861–1870. PMLR, 2018.
- [30] J. Schulman, F. Wolski, P. Dhariwal, A. Radford, and O. Klimov. Proximal policy optimization algorithms. *arXiv preprint arXiv:1707.06347*, 2017.
- [31] N. Ahmed, T. Natarajan, and K. R. Rao. Discrete cosine transform. *IEEE transactions on Computers*, 100(1):90–93, 1974.

- [32] A. Ajay, J. Wu, N. Fazeli, M. Bauza, L. P. Kaelbling, J. B. Tenenbaum, and A. Rodriguez. Augmenting physical simulators with stochastic neural networks: Case study of planar pushing and bouncing. In *2018 IEEE/RSJ International Conference on Intelligent Robots and Systems (IROS)*, pages 3066–3073. IEEE, 2018.
- [33] N. Fazeli, S. Zapolsky, E. Drumwright, and A. Rodriguez. Fundamental limitations in performance and interpretability of common planar rigid-body contact models. In *Robotics Research: The 18th International Symposium ISRR*, pages 555–571. Springer, 2020.
- [34] G. K. Wallace. The jpeg still picture compression standard. *Communications of the ACM*, 34(4):30–44, 1991.
- [35] V. Makoviychuk, L. Wawrzyniak, Y. Guo, M. Lu, K. Storey, M. Macklin, D. Hoeller, N. Rudin, A. Allshire, A. Handa, et al. Isaac gym: High performance gpu-based physics simulation for robot learning. *arXiv preprint arXiv:2108.10470*, 2021.
- [36] J. Tobin, R. Fong, A. Ray, J. Schneider, W. Zaremba, and P. Abbeel. Domain randomization for transferring deep neural networks from simulation to the real world. In *2017 IEEE/RSJ international conference on intelligent robots and systems (IROS)*, pages 23–30. IEEE, 2017.
- [37] D. Morrison, P. Corke, and J. Leitner. Egad! an evolved grasping analysis dataset for diversity and reproducibility in robotic manipulation. *IEEE Robotics and Automation Letters*, 5(3): 4368–4375, 2020.
- [38] K. Mamou, E. Lengyel, and A. Peters. Volumetric hierarchical approximate convex decomposition. In *Game Engine Gems 3*, pages 141–158. AK Peters, 2016.
- [39] J. Luntz and H. Moon. Distributed manipulation with passive air flow. In *Proceedings 2001 IEEE/RSJ International Conference on Intelligent Robots and Systems. Expanding the Societal Role of Robotics in the the Next Millennium (Cat. No. 01CH37180)*, volume 1, pages 195–201. IEEE, 2001.
- [40] A. F. Siu, E. J. Gonzalez, S. Yuan, J. B. Ginsberg, and S. Follmer. Shapeshift: 2d spatial manipulation and self-actuation of tabletop shape displays for tangible and haptic interaction. In *Proceedings of the 2018 CHI Conference on Human Factors in Computing Systems*, pages 1–13, 2018.
- [41] K. Xu, M. Qin, F. Sun, Y. Wang, Y.-K. Chen, and F. Ren. Learning in the frequency domain. In *Proceedings of the IEEE/CVF Conference on Computer Vision and Pattern Recognition*, pages 1740–1749, 2020.
- [42] Y. Xu, K. Han, C. Xu, Y. Tang, C. Xu, and Y. Wang. Learning frequency domain approximation for binary neural networks. *Advances in Neural Information Processing Systems*, 34:25553–25565, 2021.
- [43] Y. Pan, J. Mei, and A.-m. Farahmand. Frequency-based search-control in dyna. *arXiv preprint arXiv:2002.05822*, 2020.
- [44] A.-m. Farahmand. Value function in frequency domain and the characteristic value iteration algorithm. *Advances in Neural Information Processing Systems*, 32, 2019.

A More Details in Hardware Design

A.1 Robotic Frame Design

The robotic frame is shown in Figure 8. The grid cover on top is made of Acrylonitrile Butadiene Styrene plastic (ABS), using Computerized Numerical Control (CNC) for fabrication. The four surrounding sides of the shell are made of acrylic. The motor brackets and column supports are made of aluminum alloy, using CNC for production. The base is made of iron, which is welded and painted.

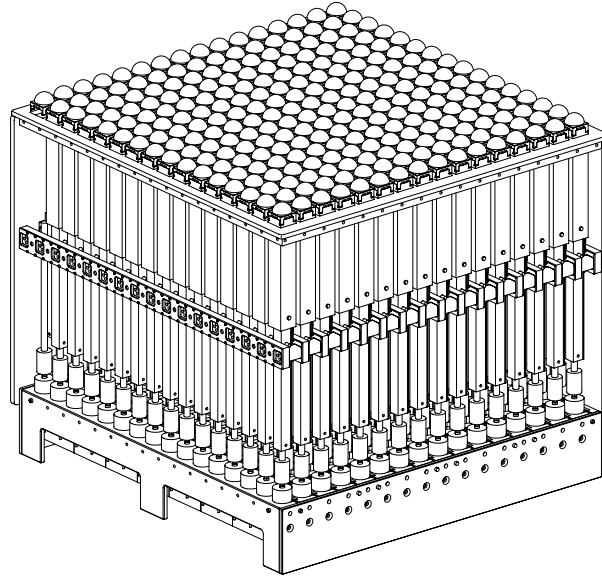


Figure 8: The robotic frame with a grid cover, a transparent shell, and an iron base.

A.2 Design and Fabrication of Pillars



Figure 9: A module of two pillars controlled by a STM32 board.

Silicone cap. To improve the transmission of force to the sensor, we develop a silicone cap with a 30A hardness. This cap is produced through vacuuming and heat setting processes. The CNC technique is also employed for producing the mold of the silicone cap.

Tactile sensor. We employ the force-sensitive resistor (FSR) sensor model RXD1016, which has a measuring range of 200 g, a resistance range of 0.5k-10k ohms, and an effective detection area of a circular shape with a diameter of 10 mm. The FSR sensor measures the normal force, and we convert the sensor resistance to voltage through a voltage divider in series. We utilize the microcontroller's Analog-to-Digital Converter (ADC) port to read the values, with the perceived pressure

being directly proportional to the voltage. As the STM32F042 board’s ADC can discern up to 0.8 mV voltage, the theoretical trigger value of the sensor is 10.36 g. In order to mitigate the impact of components such as the silicone cap on assessing the contact condition, we conduct a calibration prior to usage. This process uses the no-load voltage as the new reference zero point to evaluate the contact status.

Actuator. The DC gear motor is CHR-GM16-050ABHL, with a rated voltage of 12 V, a maximum power of 3.3 W, and a no-load speed of 800 rpm. The screw has a pitch of 1 mm and a lead of 4 mm. When the motor completes one rotation, a single column can move up by 4 mm.

Microcontroller. We select the STM32F042 microcontroller due to its inclusion of an ADC interface, a CAN interface, and an ample number of pins. Given its acceptable level of performance and relatively affordable price, this microcontroller is satisfactory for controlling ArrayBot.

Power. The robot is powered by an adjustable DC voltage source, and the power supply outputs 12 V and 5 V respectively to control the motor and the microcontroller.

B More details in RL training

RL. Our policy and value functions are separate neural networks with hidden layers of sizes [256, 256, 128]. All the inputs are normalized between 0 to 1 before feeding to the networks. We use ReLU as the activation function. We also list the hyper-parameters of PPO [30] in Table 3. The states and rewards are summarized in Table 1 and Table 2.

Training. Throughout the training phase, reinforcement learning is conducted on GPU, and the simulation is performed on CPU. Acceleration of the simulation is facilitated by using a multi-core parallel method across 128 environments. The frequency for simulation is 50 Hz, while the control frequency is 5 Hz. Training on an A40 graphics card, convergence is achieved after 10 minutes.

Table 1: A summary of all the states used in all the tasks.

Parameter	Definition	Dimension
lifting		
p	object position in World Frame	3
flipping		
θ	object orientation with axis-angle representation in world frame	3
general relocation		
p_t	object position in world frame	3
p_g	object target position in world frame	3
p_d	position difference	3
q	robot joint configuration in the frequency domain	6

Table 2: A summary of reward functions used this various tasks.

Expression	Definition	Coefficient
lifting		
$h_t - h_{t-1}$	object height difference	100
flipping		
$-\ \theta_t \cdot \theta_g^{-1}\ + \ \theta_{t-1} \cdot \theta_g^{-1}\ $	object-to-goal orientation difference	10
general relocation		
$-\ p_t - p_g\ + \ p_{t-1} - p_g\ $	object position difference	100
$\mathbb{1}\{\ p_t - p_g\ < \epsilon\}, \epsilon = 2\text{cm}$	Goal Reaching Indicator	1

Table 3: Training Hyper-parameters

Hyperparameter	Value
Discount factor	0.99
GAE parameter	0.95
Learning rate	3e-4
Environments	128
Optimizer	Adam
Normalize input	True
Normalize value	True
Normalize advantage	True

C More Details in Real-world tasks

We show more tasks that are developed using RL on ArrayBot in Figure 10. We observe that our method can generalize well to various objects, even under heavy human perturbation or visual disturbance. Additionally, we also achieve several intriguing applications by using pre-coded motion primitives on ArrayBot, as shown in Figure 11. The achieved behaviors show the potential of ArrayBot to accomplish diverse and harder tasks.



Figure 10: Applications empowered by RL-derived policies.

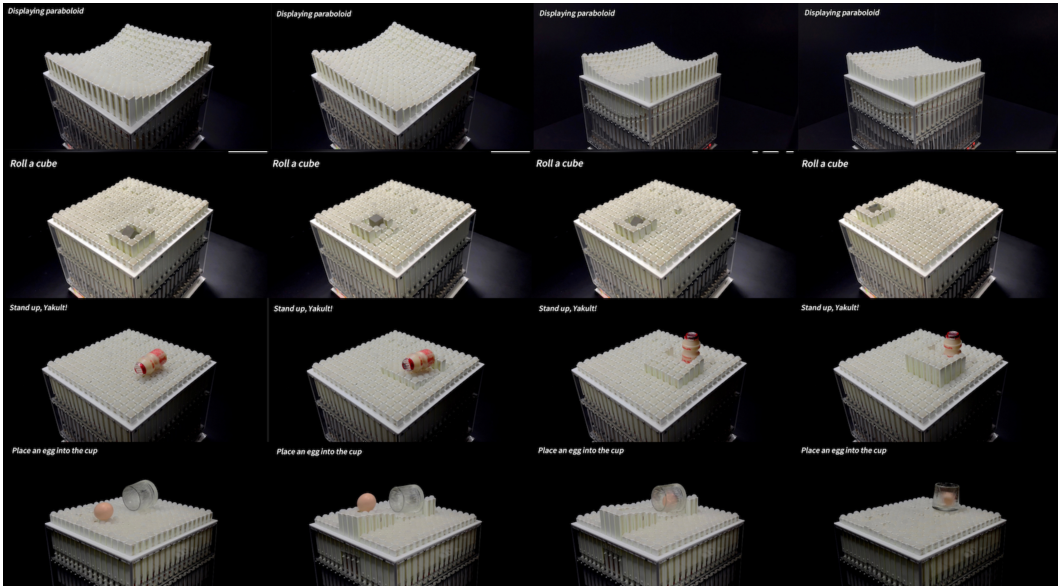


Figure 11: Applications empowered by hard-coding policies.